AIMS Geosciences, 5(3): 568–590.
DOI: 10.3934/geosci.2019.3.568
Received: 03 April 2019
Accepted: 23 July 2019
Published: 31 July 2019

http://www.aimspress.com/journal/geosciences

Research article

The significance of recent and short pluviometric time series for the assessment of flood hazard in the context of climate change: examples from some sample basins of the Adriatic Central Italy

Bufalini Margherita[1,*], Farabollini Piero[1], Fuffa Emy[1], Materazzi Marco[1], Pambianchi Gilberto[1] and Tromboni Michele[2]

[1] University of Camerino, School of Science and Technology-Geology Division, Via Gentile III da Varano, Camerino (MC) 62032, Italy
[2] Consorzio di Bonifica delle Marche, Sede Legale Via Guidi, 39, 61121 Pesaro, Italy

* **Correspondence:** Email: margherita.bufalini@unicam.it; Tel: +393384842780.

Abstract: Numerical hydrological models are increasingly a fundamental tool for the analysis of floods in a river basin. If used for predictive purposes, the choice of the "design storm" to be applied, once set other variables (as basin geometry, land use, etc.), becomes fundamental.

All the statistical methods currently adopted to calculate the design storm, suggest the use of long rainfall series (at least 40–50 years). On the other hand, the increasingly high frequency of intense events (rainfalls and floods) in the last twenty years, also as a result of the ongoing climate change, testify to the need for a critical analysis of the statistical significance of these methods.

The present work, by applying the Gumbel distribution (Generalized Extreme Value Type-I distribution) on two rainfall series (1951–2018 and 1998–2018) coming from the same rain gauges and the "Chicago Method" for the calculation of the design storm, highlights how the choice of the series may influence the formation of flood events.

More in particular, the comparison of different hydrological models, generated using HEC-HMS software on three sample basins of the Adriatic side of central Italy, shows that the use of shorter and recent rainfall series results in a generally higher runoff, mostly in case of events with a return time equal or higher than 100 years.

Keywords: flood hazard; design storm; HEC-HMS model; climatic change; 2007/60/EC-Flood Directive (FD); central Italy

1. Introduction

Climate is undoubtedly the principal driving force in hydrologic systems. Nevertheless, the significant increase of floods observed in many regions of the world is often attributed to land use change, while the climate forcing under the effects of increased atmospheric greenhouse gases is usually underestimated.

At the end of 2018 the Intergovernmental Panel on Climate Change [1] published a "Special Report" on the impacts of 1.5 °C global warming above pre-industrial levels and related global greenhouse gas emission pathways, contained in the Decision of the 21st Conference of Parties of the United Nations Framework Convention on Climate Change to adopt the Paris Agreement. According to this Report, climate change is expected to increase extreme precipitations over many countries of Europe and, consequently, the risk of flooding on urban areas or rivers.

Even the Directive 2007/60/EC of the European Parliament and of the Council of 23 October 2007 (Directive "Floods"—FD), adopted with the aim of assess and manage flood risk, aims at the reduction of the harmful impacts on human health, environment, cultural heritage and economic activities. In particular, the article 4, paragraph 2 of the Directive states that "Based on available or readily derivable information, such as records and studies on long term developments, in particular impacts of climate change on the occurrence of floods, a preliminary flood risk assessment shall be undertaken to provide an assessment of potential risks".

The preparation of flood hazard and flood risk maps play and a key role in the implementation of the Directive itself and all the Member States, before the deadline of 22 December 2013, had to make maps at the most appropriate scale for selected areas, according to different climatic probability scenarios. Nevertheless, even though many States completed the procedure in time, several studies carried out in recent years [2,3] evidenced that the proposed scenarios, in the light of the ongoing climate change, are in some cases unrealistic, especially with regard to very extreme events (associated to long return time). The cause is certainly to be found, in addition to the consequences linked to the land use changes on the slopes and to the anthropization of alluvial plains and riverbeds, to the increase of intense rainfall events during the last twenty years, sometimes related (in densely populated areas) to urban growth-driven, microclimatic change (urban heat islands).

The hydrological models currently used for the definition of flood hazard scenarios, involve the use of different formulas and algorithms for the calculation of the "net rain" and for the definition of the "rainfall-runoff transformation process". Nevertheless, if the choice of the method or algorithm can produce different but substantially comparable results, the definition of the best "design storm", (i.e. the rainfall event that is expected to occur in the considered site for a given probability of occurrence and a given duration of the storm) obtained through statistical-probabilistic approaches, results critical.

The present study, by applying the Chicago-type hyetograph (considered representative of the design storm for the study area) to 18 rain gauges belonging to three sample basins of the Adriatic side of central Italy, highlights how the calculation of the hyetograph itself carried out by analyzing historical rainfalls series of different length, gives rise to significantly different results when used as input in a hydrological model for the calculation of the peak of flow along a river basin. Comparing the peak flow rates generated using a Chicago hyetograph derived from a "long" time series (about 70 years, from 1951 to 2018) and from a more recent part of it (about 20 years, 1998–2018) emerges

as the latter produces in most cases higher flow rates. Although the result may appear less reliable from a statistical point of view, this aspect is instead important in a context of climate change, such as the current one, in which extreme events occur with ever more frequency.

2. Materials and method

2.1. Geological, geomorphological and climatic context

The study area (around 2600 km^2), which includes the Musone (651 km^2), Esino (1219 km^2) and Potenza (775 km^2) river basins, encompasses a wide territory of the Adriatic side of Central Italy, characterized by a typical mountain/high-hilly landscape in the central-western portion and few flat sectors located along the main alluvial plains and eastward, near the coast (Figure 1).

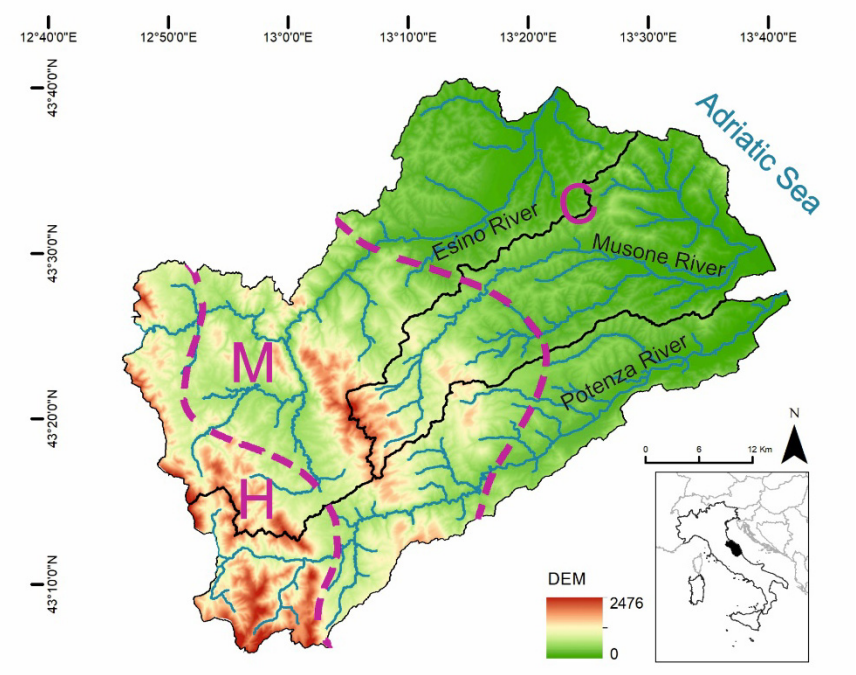

Figure 1. Location of the study area: H = high-hilly and mountain sector, M = intermediate medium-low hilly sector, C = coastal sector.

More in detail, it can be generally divided into three longitudinal sectors, homogeneous in the range of altitudes and for their lithological (Figure 2a) and climatic (Figure 2b) characters [4−6]:

- a coastal sector (C), between 0m and 537m a.s.l. characterized by a clayey-sandy-conglomeratic bedrock and mean annual precipitation between 600 mm and 850 mm;
- an intermediate medium-low hilly sector (M), between 95m and 1475m a.s.l. with mainly arenaceous-conglomeratic and sandy-pelitic bedrock and mean annual precipitation between 850 mm and 1100 mm;

- an inner high-hilly and mountain sector (H), between 271 m and 1692 m a.s.l with the presence of mainly calcareous lithotypes and mean annual rainfalls between 1100 mm, and 1700 mm.

The trend of the average monthly temperatures and rainfalls, over the entire study area (calculated over the period 1950–2018) is shown in Figure 3.

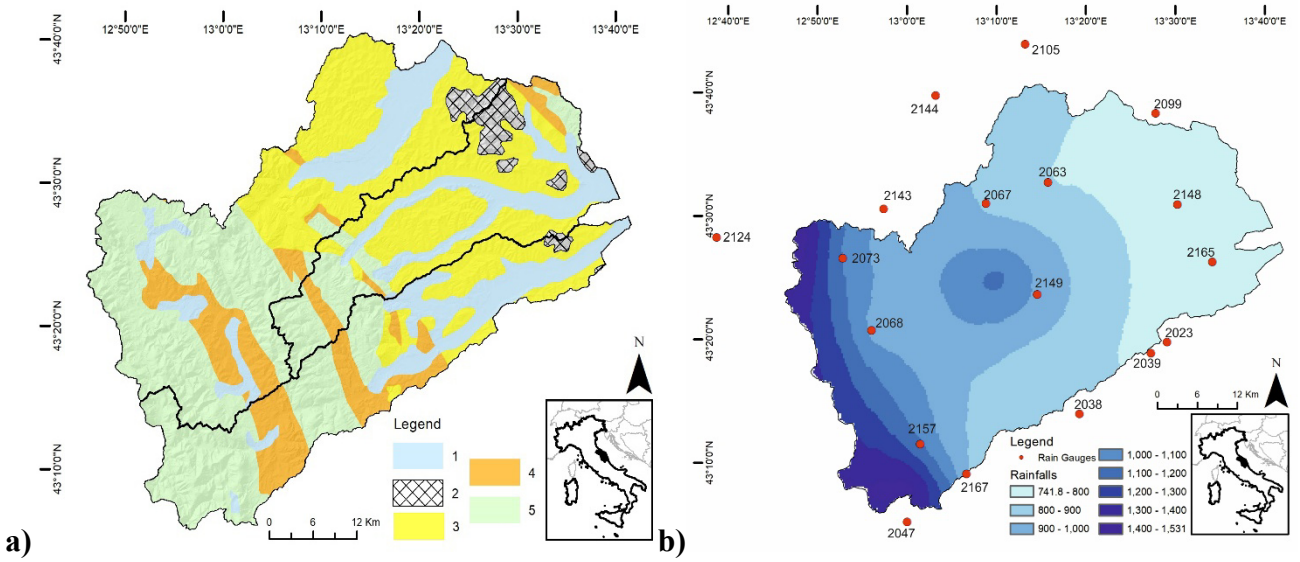

Figure 2. a) Schematic geological map of the Marche region. 1 = Main continental deposits (Pliocene-Pleistocene-Holocene); 2 = Sands and conglomerates (Pliocene-Pleistocene); 3 = Clays and sands (Pliocene-Pleistocene; 4 = Arenaceous-marly-clayey turbidites (late Miocene); 5 = Limestones, marly limestones and marls (early Jurassic-Oligocene). b) Mean annual precipitation map of the Marche region. Larger symbols for the rain gauges indicate those employed in the hydrological model.

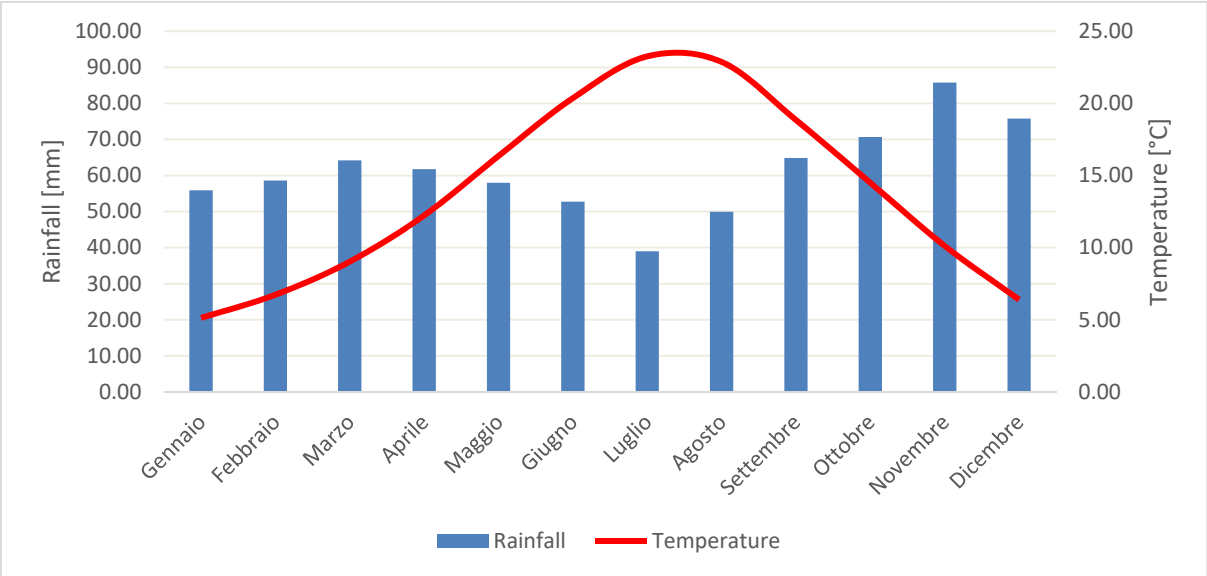

Figure 3. Histogram of the average monthly temperature and rainfalls.

Such climatic features characterize what is currently defined as "Adriatic-sublitorial" regime [4]. The number of rainy days in this sector ranges between 60 and 75 while the daily mean intensity between 10 and 12 mm; the absolute monthly maximum is usually in November (secondary maximum in spring). Summer is rather dry, particularly near the coast, where periods without rainfall exceed 40 days. The mean annual temperatures on the other hand vary between 12.5 °C and 15.5 °C; the annual temperature excursion is around 18 °C, while the daily one goes from 7 °C along the coast to 10 °C in the intramountain basins. The Aridity Index—AI values varies from 19.9 to 38, defining an area which presents an average, slight summer aridity in the littoral portion and the low hills. The Modified Fournier erosivity Index—MFI ranges from 8.2. to 9.6 indicating a low erosion potential.

2.2. Rainfall data analysis

Hydrological modelling, as known, requires the definition of design storms or precipitation hyetographs. Design storms are then used as inputs to hydrological models, while the resulting flows and flow rates in a river basin are calculated using rainfall-runoff and flow routing procedures.

The present study calculates the design storm following the "Chicago Method". This method establishes two different analytical equations for rainfall intensity over time, one valid before and another one valid after the peak rate, both derived from a Depth-Duration-Frequency (DDF) analytical expression, that preserves the same volumes of all rainfall intensities. Intensity-Duration-Frequency (DDF) curves, on the other hand, express in a synthetic way, for a given return time (T) (or its inverse, probability of exceedance) and a duration (t) of a rainfall event, the information on the maximum height of precipitation (h) and the maximum rainfall intensity (i). Generally, DDF curves can be described by the expression:

$$h(t,T) = at^n \tag{1}$$

in which a and n are parameters that have to be estimated through a probabilistic approach.

The cumulative probability function F_X (x) represents the probability of not exceeding the value of the rainfall height h by that random variable. In this study, the cumulative distribution function used was the classical Generalized Extreme Value (GEV) Type-I distribution (or Gumbel distribution)

$$F_X(x) = exp\{-exp[(x-\xi)/\alpha]\} \tag{2}$$

where X is a random variable, x is a possible value of X, ξ is the location parameter calculated using $\mu_X = \xi + 0.5772\alpha$ and α is the scale parameter calculated using $\sigma_X^2 = \pi^2\alpha^2/6$, where μ_X is the mean and σ_X^2 the variance of the data set [7,8].

Rainfall data used in this study come from 18 weather stations, managed by the Marche Region Multi-risk Functional Center and considered representatives of the area analyzed (Figure 4). These weather station (whose characteristic parameters are given in Table 1) are distributed as follows:

- 10 in the coastal sector;
- 4 in the medium and low-hilly sector;
- 4 in the high-hilly and mountainous sector.

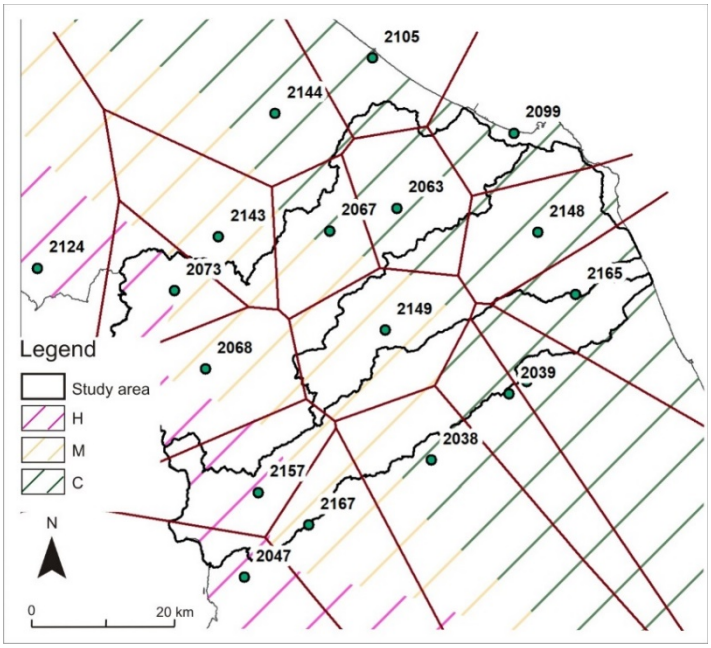

Figure 4. Location of the study area with indication of the rain gauges used for the statistical analysis. The map also shows the subdivision into areas of equal height of precipitation, processed through the Thiessen polygon method and the subdivision into climatic macro-areas: H = high-hilly and mountain sector, M = intermediate medium-low hilly sector, C = coastal sector.

Table 1. List of the rain gauges used in the study.

Rain Gauge	Gauge ID	Zone	x coord (m)	y coord (m)	Elevation (m a.s.l.)	Missing Years (1950–2018)	Missing Years (1998–2018)
Macerata	2023	C	2394389	4795201	280	-	-
Tolentino	2038	C	2380482	4785380	244	-	-
Macerata	2039	C	2391814	4793706	232	-	-
Jesi	2063	C	2378238	4820428	96	4	-
Maiolati Spontini	2067	C	2368749	4817949	110	1	-
Ancona	2099	C	2395140	4829598	6	15	-
Senigallia	2105	C	2376352	4841364	5	11	-
Osimo	2148	C	2397421	4815699	265	30	-
Recanati	2165	C	2402028	4806729	235	6	-
Fabriano	2068	M	2350190	4800177	357	1	-
Arcevia	2143	M	2353319	4818252	535	-	-
Corinaldo	2144	M	2362356	4834672	203	40	-
Cingoli	2149	M	2375411	4803758	631	5	1
Camerino	2167	M	2362874	4777647	664	29	9
Serravalle di Chienti	2047	H	2353490	4771078	647	40	-
Sassoferrato	2073	H	2346666	4811257	312	40	-
Cantiano	2124	H	2328006	4815746	360	-	-
Pioraco	2157	H	2356279	4782617	441	2	-

To calculate the design storms, the maximum rainfall values recorded each year for durations of 1, 3, 6, 12 and 24 hours were collected for each rain gauge and, where available, for the period 1950–2018.

To verify the existence of a positive or negative trend of rainfall data and their statistical significance, the non-parametric Mann-Kendall and Sen's slope estimator tests, very frequently used for the analysis of hydro-meteorological time series[9,10], were performed on both the "long" (1950–2018) and "short" (1998–2018) periods, to check also for possible changings.

The Mann-Kendall test S is generally calculated as:

$$S = \sum_{i=1}^{n-1} \sum_{j=i+1}^{n} sgn(x_j - x_i) \tag{3}$$

where n is the number of data points, x_i and x_j are the data values in time series i and j ($j > i$), respectively and $sgn(x_j - x_i)$ is the sign function as:

$$sgn(x_j - x_j) = \begin{cases} +1, if\ x_j - x_i > 0 \\ 0, if\ x_j - x_i = 0 \\ -1, if\ x_j - x_i < 0 \end{cases} \tag{4}$$

The variance is calculated as:

$$Var(S) = \frac{n(n-1)(2n+5) - \sum_{i=1}^{m} t_i(t_i-1)(2t_i+5)}{18} \tag{5}$$

where n is the number of data, m is the number of tied groups (i.e. sets of sample data having the same value) and t_i is the number of ties of extent i. In cases where the sample size $n > 10$, the standard normal test statistic Z is computed as follows:

$$Z = \begin{cases} \frac{S-1}{\sqrt{Var(S)}}, if\ S > 0 \\ 0 \quad if\ S = 0 \\ \frac{S-1}{\sqrt{Var(S)}}, if\ S < 0 \end{cases} \tag{6}$$

Positive values of Z indicate increasing trends while negative Z values show decreasing trends. Testing trends is usually done at a specific significance level. In this study, significance levels of 99% and 95% were used.

The *Sen's slope estimator* test (Q) describes the slope of trend in the sample of N pairs of data:

$$Q = \frac{x_j - x_k}{j - k}\ for\ i = 1, \ldots . N, \tag{7}$$

where x_j and x_k are the data values at times j and k ($j > k$), respectively.

The Q sign evidences data trend reflection, while its value indicates the steepness of the trend. To determine whether the slope is statistically different than zero, one should calculate the

confidence interval of Q at specific probability; same as for the Mann-Kendall test, significance levels of 99% and 95% have been chosen.

The results of the tests have shown in Table 2. From the analysis of results it is evident that only some weather stations register statistically significant trends; nevertheless, the latter always show a positive trend and the number of stations systematically increases (for all the durations analyzed) in the "short" period (1998–2018).

After this step, rainfall data were subsequently subjected to statistical analysis using the GEV Type I distribution to obtain the DDF curves. The spatialization of rainfall data over the whole study area functional to the use within the hydrologic model, has been finally implemented using the "Thiessen polygons" method [11]. Although other methods are also commonly used for the spatial distribution of rainfall data, the choice was here forced due to the software used for the hydrological modeling. As will be explained in more detail below, the association of specific design storm to each weather station within HEC-HMS, can only be achieved using the aforementioned tool; other methods only allow the insertion of a single maximum rainfall height, a procedure considered less suitable also for the successive calibration carried out with the observed river flow data.

Table 2A. Results of the statistical analysis carried out on different time series (1950–2018; 1998–2018) and durations. (1 hour 1950–2018).

Rain Gauge Code	First year	Last Year	n	Test Z	Signif.	Q	Qmin99	Qmax99	Qmin95	Qmax95
2023	1950	2018	20	0.28		0.013	−0.150	0.180	−0.105	0.143
2038	1950	2018	20	0.30		0.018	−0.159	0.200	−0.120	0.158
2039	1950	2018	21	−0.07		0.000	−0.161	0.157	−0.129	0.114
2063	1950	2018	18	1.10		0.052	−0.083	0.167	−0.053	0.142
2067	1950	2018	21	−1.23		-0.057	−0.185	0.080	−0.146	0.042
2099	1950	2018	21	0.21		0.005	−0.114	0.153	−0.082	0.122
2105	1950	2018	21	1.52		0.108	−0.076	0.295	−0.030	0.250
2148	1950	2018	20	0.76		0.048	−0.178	0.242	−0.101	0.183
2165	1950	2018	21	−0.77		-0.047	−0.206	0.111	−0.172	0.067
2068	1950	2018	19	−0.69		-0.040	−0.201	0.117	−0.157	0.074
2143	1950	2018	21	−0.05		0.000	−0.147	0.144	−0.109	0.100
2144	1950	2018	21	−0.14		-0.046	−0.612	0.517	−0.436	0.400
2149	1950	2018	20	0.72		0.045	−0.109	0.207	−0.075	0.167
2167	1950	2018	11	−0.28		-0.015	−0.262	0.124	−0.210	0.087
2047	1950	2018	20	−0.98		-0.046	−0.171	0.083	−0.144	0.051
2073	1950	2018	21	1.82	X	0.380	−0.170	1.094	−0.037	0.953
2124	1950	2018	21	1.16		0.054	−0.064	0.188	−0.039	0.155
2157	1950	2018	21	1.31		0.062	−0.063	0.184	−0.027	0.157

Table 2B. Results of the statistical analysis carried out on different time series (1950–2018; 1998–2018) and durations. (1 hour 1998–2018).

Rain Gauge Code	First year	Last Year	n	Test Z	Signif.	Q	Qmin99	Qmax99	Qmin95	Qmax95
2023	1998	2018	20	2.47	X	1.164	−0.033	2.468	0.331	2.099
2038	1998	2018	20	2.50	X	1.207	−0.088	1.875	0.372	1.693
2039	1998	2018	21	2.30	X	0.955	−0.079	2.278	0.220	1.783
2063	1998	2018	21	0.06		0.000	−0.622	0.984	−0.400	0.600
2067	1998	2018	21	1.12		0.514	−0.310	1.382	−0.143	1.146
2099	1998	2018	21	1.21		0.310	−0.523	1.164	−0.135	0.922
2105	1998	2018	21	2.14	X	0.981	−0.328	2.567	0.119	1.869
2148	1998	2018	20	0.23		0.045	−1.066	0.873	−0.683	0.641
2165	1998	2018	21	1.18		0.414	−0.777	1.480	−0.360	1.234
2068	1998	2018	19	0.67		0.200	−0.612	0.959	−0.443	0.825
2143	1998	2018	21	−0.79		−0.219	−1.425	0.818	−1.200	0.448
2144	1998	2018	21	−0.15		−0.067	−1.078	0.911	−0.863	0.717
2149	1998	2018	20	1.53		0.451	−0.483	1.416	−0.105	1.112
2167	1998	2018	11	−0.70		−0.720	−6.473	2.598	−5.605	1.025
2047	1998	2018	20	1.04		0.406	−0.577	1.142	−0.425	0.942
2073	1998	2018	21	2.08	X	0.900	−0.247	2.072	0.044	1.572
2124	1998	2018	21	−0.03		−0.025	−1.158	0.969	−0.948	0.714
2157	1998	2018	21	0.00		0.000	−0.795	0.867	−0.578	0.628

Table 2C. Results of the statistical analysis carried out on different time series (1950–2018; 1998–2018) and durations. (3 hours 1950–2018).

Rain Gauge Code	First year	Last Year	n	Test Z	Signif.	Q	Qmin99	Qmax99	Qmin95	Qmax95
2023	1950	2018	68	1.21		0.092	−0.104	0.284	−0.050	0.235
2038	1950	2018	66	0.20		0.017	−0.163	0.240	−0.114	0.173
2039	1950	2018	68	1.02		0.077	−0.100	0.261	−0.065	0.205
2063	1950	2018	65	0.97		0.073	−0.138	0.270	−0.086	0.207
2067	1950	2018	68	−0.65		−0.050	−0.222	0.147	−0.183	0.095
2099	1950	2018	52	−0.22		−0.020	−0.245	0.196	−0.197	0.127
2105	1950	2018	58	0.76		0.083	−0.181	0.400	−0.112	0.333
2148	1950	2018	36	1.01		0.059	−0.177	0.400	−0.086	0.309
2165	1950	2018	64	0.00		0.000	−0.224	0.200	−0.161	0.148
2068	1950	2018	66	−0.18		−0.015	−0.228	0.154	−0.164	0.120
2143	1950	2018	69	0.92		0.063	−0.107	0.245	−0.067	0.200
2144	1950	2018	28	−0.26		−0.086	−0.880	0.792	−0.648	0.585
2149	1950	2018	65	1.09		0.091	−0.139	0.312	−0.079	0.255
2167	1950	2018	38	−0.24		−0.021	−0.271	0.177	−0.213	0.117
2047	1950	2018	50	−0.24		−0.021	−0.227	0.194	−0.168	0.136
2073	1950	2018	28	0.43		0.110	−0.535	1.162	−0.387	0.805
2124	1950	2018	69	0.47		0.030	−0.146	0.200	−0.102	0.160
2157	1950	2018	67	2.00	X	0.109	−0.030	0.233	0.000	0.200

Table 2D. Results of the statistical analysis carried out on different time series (1950–2018; 1998–2018) and durations. (3 hours 1998–2018).

Rain Gauge Code	First year	Last Year	n	Test Z	Signif.	Q	Qmin99	Qmax99	Qmin95	Qmax95
2023	1998	2018	20	2.82	X	1.51	0.116	2.951	0.465	2.539
2038	1998	2018	20	1.88	X	0.76	−0.400	2.325	−0.056	1.800
2039	1998	2018	21	2.63	X	1.23	0.041	2.600	0.304	2.230
2063	1998	2018	18	0.98		0.78	−1.171	3.145	−0.694	2.209
2067	1998	2018	21	1.99	X	0.73	−0.216	1.982	0.020	1.708
2099	1998	2018	21	0.06		0.03	−1.745	1.239	−1.020	0.855
2105	1998	2018	21	1.15		0.95	−1.058	2.933	−0.808	2.535
2148	1998	2018	20	0.81		0.267	−0.822	1.540	−0.468	1.200
2165	1998	2018	21	1.18		0.558	−1.161	1.982	−0.620	1.648
2068	1998	2018	19	0.42		0.250	−1.646	1.266	−0.883	1.087
2143	1998	2018	21	−1.24		−0.527	−1.688	0.611	−1.330	0.363
2144	1998	2018	21	0.60		0.269	−0.815	1.669	−0.587	1.325
2149	1998	2018	20	1.40		0.729	−0.638	1.813	−0.210	1.555
2167	1998	2018	11	−1.33		−1.533	−6.298	1.854	−5.464	1.134
2047	1998	2018	20	0.26		0.200	−1.010	1.162	−0.733	1.000
2073	1998	2018	21	1.69	X	0.530	−0.400	2.583	−0.103	1.936
2124	1998	2018	21	1.03		0.329	−0.795	1.433	−0.422	1.000
2157	1998	2018	21	−0.03		−0.029	−0.937	0.918	−0.731	0.682

Table 2E. Results of the statistical analysis carried out on different time series (1950–2018; 1998–2018) and durations. (6 hours 1950–2018).

Rain Gauge Code	First year	Last Year	n	Test Z	Signif.	Q	Qmin99	Qmax99	Qmin95	Qmax95
2023	1950	2018	68	1.65	X	0.143	−0.078	0.356	−0.026	0.291
2038	1950	2018	66	1.81	X	0.138	−0.057	0.370	−0.014	0.318
2039	1950	2018	68	1.59		0.122	−0.067	0.319	−0.025	0.260
2063	1950	2018	65	0.91		0.084	−0.144	0.336	−0.082	0.255
2067	1950	2018	68	−0.20		−0.013	−0.214	0.164	−0.167	0.120
2099	1950	2018	52	−0.73		−0.083	−0.385	0.205	−0.314	0.136
2105	1950	2018	58	1.04		0.149	−0.168	0.467	−0.110	0.400
2148	1950	2018	36	1.28		0.139	−0.181	0.467	−0.083	0.369
2165	1950	2018	64	0.28		0.033	−0.208	0.266	−0.147	0.200
2068	1950	2018	66	−0.13		−0.005	−0.190	0.161	−0.143	0.117
2143	1950	2018	69	1.16		0.082	−0.107	0.294	−0.057	0.243
2144	1950	2018	28	0.00		0.000	−1.051	1.040	−0.763	0.734
2149	1950	2018	65	0.99		0.108	−0.155	0.356	−0.100	0.289
2167	1950	2018	38	0.72		0.069	−0.230	0.350	−0.153	0.253
2047	1950	2018	50	0.36		0.030	−0.192	0.227	−0.143	0.176
2073	1950	2018	28	0.38		0.117	−0.582	1.894	−0.405	1.395
2124	1950	2018	69	0.68		0.047	−0.150	0.263	−0.100	0.200
2157	1950	2018	67	2.538	X	0.178	−0.002	0.382	0.056	0.334

Table 2F. Results of the statistical analysis carried out on different time series (1950–2018; 1998–2018) and durations. (6 hours 1998–2018).

Rain Gauge Code	First year	Last Year	n	Test Z	Signif.	Q	Qmin99	Qmax99	Qmin95	Qmax95
2023	1998	2018	20	1.95	X	1.050	−0.290	2.858	−0.004	2.465
2038	1998	2018	20	1.46		0.939	−0.637	2.172	−0.338	1.981
2039	1998	2018	21	1.45		0.719	−0.624	2.600	−0.192	2.200
2063	1998	2018	18	1.29		0.860	−0.979	3.406	−0.556	2.592
2067	1998	2018	21	2.78	X	0.898	0.100	2.127	0.277	1.849
2099	1998	2018	21	−0.27		−0.194	−2.837	1.623	−2.311	1.072
2105	1998	2018	21	1.18		1.077	−1.339	3.365	−0.623	2.778
2148	1998	2018	20	0.58		0.253	−1.323	1.800	−0.893	1.412
2165	1998	2018	21	0.57		0.440	−1.288	2.113	−0.720	1.737
2068	1998	2018	19	−0.07		−0.010	−1.676	0.832	−0.722	0.600
2143	1998	2018	21	−0.94		−0.447	−1.703	1.051	−1.306	0.687
2144	1998	2018	21	0.94		0.510	−0.815	1.846	−0.533	1.600
2149	1998	2018	20	1.8828	X	0.914	−0.333	2.485	−0.057	1.933
2167	1998	2018	11	−0.93		−1.489	−5.885	4.135	−4.599	1.393
2047	1998	2018	20	0.13		0.075	−1.167	1.306	−0.736	0.960
2073	1998	2018	21	1.27		0.640	−0.547	3.896	−0.255	3.180
2124	1998	2018	21	0.97		0.544	−1.150	1.580	−0.605	1.333
2157	1998	2018	21	0.82		0.289	−1.098	2.196	−0.741	1.781

Table 2G. Results of the statistical analysis carried out on different time series (1950–2018; 1998–2018) and durations. (12 hours 1950–2018).

Rain Gauge Code	First year	Last Year	n	Test Z	Signif.	Q	Qmin99	Qmax99	Qmin95	Qmax95
2023	1950	2018	68	1.86	X	0.184	−0.071	0.504	−0.008	0.400
2038	1950	2018	66	2.24	X	0.261	−0.039	0.521	0.022	0.450
2039	1950	2018	68	1.07		0.120	−0.161	0.421	−0.095	0.342
2063	1950	2018	65	1.59		0.139	−0.108	0.388	−0.049	0.320
2067	1950	2018	68	0.35		0.034	−0.212	0.274	−0.154	0.225
2099	1950	2018	52	−0.47		−0.056	−0.368	0.248	−0.280	0.173
2105	1950	2018	58	1.24		0.158	−0.188	0.486	−0.110	0.396
2148	1950	2018	36	1.23		0.165	−0.206	0.650	−0.112	0.518
2165	1950	2018	64	0.53		0.061	−0.263	0.359	−0.183	0.283
2068	1950	2018	66	0.06		0.005	−0.217	0.235	−0.158	0.167
2143	1950	2018	69	1.16		0.109	−0.124	0.350	−0.074	0.288
2144	1950	2018	28	0.16		0.106	−1.436	1.207	−0.922	0.924
2149	1950	2018	65	0.03		0.003	−0.302	0.310	−0.230	0.242
2167	1950	2018	38	0.68		0.081	−0.254	0.445	−0.170	0.347
2047	1950	2018	50	0.20		0.015	−0.200	0.221	−0.156	0.177
2073	1950	2018	28	1.46		0.576	−0.387	2.206	−0.120	1.822
2124	1950	2018	69	0.86		0.115	−0.231	0.462	−0.137	0.367
2157	1950	2018	67	2.58	X	0.216	0.000	0.460	0.055	0.400

Table 2H. Results of the statistical analysis carried out on different time series (1950–2018; 1998–2018) and durations. (12 hours 1998–2018).

Rain Gauge Code	First year	Last Year	n	Test Z	Signif.	Q	Qmin99	Qmax99	Qmin95	Qmax95
2023	1998	2018	20	1.07		1.034	−1.208	3.624	−0.642	3.147
2038	1998	2018	20	1.27		0.790	−1.133	2.820	−0.513	2.655
2039	1998	2018	21	0.51		0.588	−1.538	3.220	−1.106	2.478
2063	1998	2018	18	2.35	X	1.600	−0.156	3.020	0.467	2.605
2067	1998	2018	21	2.39	X	1.215	−0.213	2.400	0.286	2.057
2099	1998	2018	21	−0.48		−0.335	−2.736	1.562	−1.838	1.056
2105	1998	2018	21	1.36		1.247	−1.447	3.343	−0.751	3.065
2148	1998	2018	20	0.19		0.090	−2.298	2.761	−1.716	2.253
2165	1998	2018	21	0.73		0.445	−1.805	2.585	−1.133	2.035
2068	1998	2018	19	0.11		0.038	−2.400	1.741	−1.679	1.290
2143	1998	2018	21	−0.73		−0.335	−1.764	1.645	−1.452	1.018
2144	1998	2018	21	1.39		0.547	−0.563	2.863	−0.232	2.129
2149	1998	2018	20	1.36		0.883	−0.757	3.059	−0.393	2.577
2167	1998	2018	11	−0.31		−1.267	−10.606	6.516	−7.341	5.199
2047	1998	2018	20	−0.13		−0.049	−1.745	1.636	−1.338	1.007
2073	1998	2018	21	1.78	X	1.183	−0.400	4.731	−0.080	3.713
2124	1998	2018	21	0.85		0.646	−1.574	3.049	−0.928	2.634
2157	1998	2018	21	0.82		0.452	−1.000	2.646	−0.700	2.218

Table 2I. Results of the statistical analysis carried out on different time series (1950–2018; 1998–2018) and durations. (24 hours 1950–2018).

Rain Gauge Code	First year	Last Year	n	Test Z	Signif.	Q	Qmin99	Qmax99	Qmin95	Qmax95
2023	1950	2018	68	1.94	X	0.244	−0.104	0.620	−0.001	0.524
2038	1950	2018	66	1.59		0.257	−0.161	0.579	−0.058	0.491
2039	1950	2018	68	1.34		0.168	−0.172	0.530	−0.078	0.439
2063	1950	2018	65	1.06		0.104	−0.176	0.372	−0.092	0.316
2067	1950	2018	68	0.16		0.025	−0.279	0.298	−0.200	0.218
2099	1950	2018	52	−0.94		−0.142	−0.506	0.270	−0.416	0.169
2105	1950	2018	58	0.91		0.116	−0.273	0.426	−0.183	0.349
2148	1950	2018	36	2.10	X	0.310	−0.096	1.000	0.011	0.766
2165	1950	2018	64	0.83		0.136	−0.275	0.554	−0.189	0.435
2068	1950	2018	66	0.33		0.026	−0.220	0.289	−0.155	0.225
2143	1950	2018	69	1.37		0.139	−0.139	0.403	−0.077	0.333
2144	1950	2018	28	0.87		0.342	−1.089	1.618	−0.574	1.247
2149	1950	2018	65	0.00		0.000	−0.372	0.370	−0.278	0.275
2167	1950	2018	38	1.12		0.172	−0.244	0.550	−0.135	0.451
2047	1950	2018	50	−0.69		−0.063	−0.347	0.200	−0.273	0.146
2073	1950	2018	28	1.74	X	0.897	−0.526	2.546	−0.146	2.078
2124	1950	2018	69	0.95		0.169	−0.284	0.654	−0.169	0.518
2157	1950	2018	67	2.57	X	0.281	0.000	0.561	0.076	0.498

Table 2J. Results of the statistical analysis carried out on different time series (1950–2018; 1998–2018) and durations. (24 hours 1998–2018).

Rain Gauge Code	First year	Last Year	n	Test Z	Signif.	Q	Qmin99	Qmax99	Qmin95	Qmax95
2023	1998	2018	20	2.04	X	2.142	−0.817	4.618	0.154	3.927
2038	1998	2018	20	1.07		1.167	−2.256	4.127	−1.025	3.371
2039	1998	2018	21	1.36		1.458	−2.196	4.115	−0.836	3.295
2063	1998	2018	18	2.77	X	2.067	0.140	3.714	0.628	3.367
2067	1998	2018	21	1.90	X	1.242	−0.491	3.398	−0.054	2.733
2099	1998	2018	21	−0.42		−0.182	−2.917	2.333	−1.908	1.549
2105	1998	2018	21	1.54		1.297	−1.308	4.232	−0.479	3.467
2148	1998	2018	20	0.58		0.255	−3.248	3.444	−2.491	2.879
2165	1998	2018	21	1.18		1.437	−2.028	5.096	−1.301	4.431
2068	1998	2018	19	−0.14		−0.080	−2.371	1.733	−1.827	1.302
2143	1998	2018	21	−0.57		−0.257	−1.747	2.554	−1.444	1.660
2144	1998	2018	21	1.75	X	0.927	−0.531	3.520	−0.086	2.695
2149	1998	2018	20	1.10		0.825	−1.643	3.900	−0.720	3.092
2167	1998	2018	11	−0.39		−0.950	−13.199	11.285	−11.074	4.885
2047	1998	2018	20	−1.07		−0.688	−3.075	1.207	−2.624	0.678
2073	1998	2018	21	1.87	X	1.745	−0.827	4.837	−0.200	3.832
2124	1998	2018	21	0.57		0.452	−2.432	4.635	−1.881	3.296
2157	1998	2018	21	1.48		0.811	−0.914	3.133	−0.427	2.792

2.3. Land use

Concerning the land use, vector data from the IIIrd level of the CORINE Land Cover 2012 inventory (CLC-2012)[12] have been collected (Figure 5a); the analysis of data, evidences that around 68% is characterized by agricultural areas, 27% by Forest and Seminatural areas and only 5% by Artificial surfaces. The characteristics of the soils, on the other hand, have been extrapolated generalizing and integrating data from the Soil Map of the Marche Region at 1: 250,000 scale. The different types of soil have been merged according to the World Reference Base for Soil Resources—WRB [13]. Four main groups of the WRB characterize the study area: Cambisols, Leptosols, Regosols, Calcisols.

Cambisols, very common in temperate and boreal regions, are brownish soils with weak horizon differentiation and characterized by the presence of a cambic horizon (Bw), below the organic-mineral one. These soils are predominant in the sedimentary basin placed within the calcareous ridges of the Apennine chain. Leptosols are very shallow soils with minimal development, formed typically on hard rock or highly calcareous materials; in the study area they are present along the Apennine ridges and are mainly developed over colluvial and slope quaternary deposits. Regosols, mostly developed along the alluvial plains, are usually not shallow enough to be Leptosols and consist of very weakly developed mineral soils in unconsolidated materials with only an ochric surface horizon. Calcisols, finally, are soils with a significant secondary accumulation of calcium carbonate and are common on the low-hilly areas of the region where a mainly pelitic and sandy-pelitic bedrock outcrops.

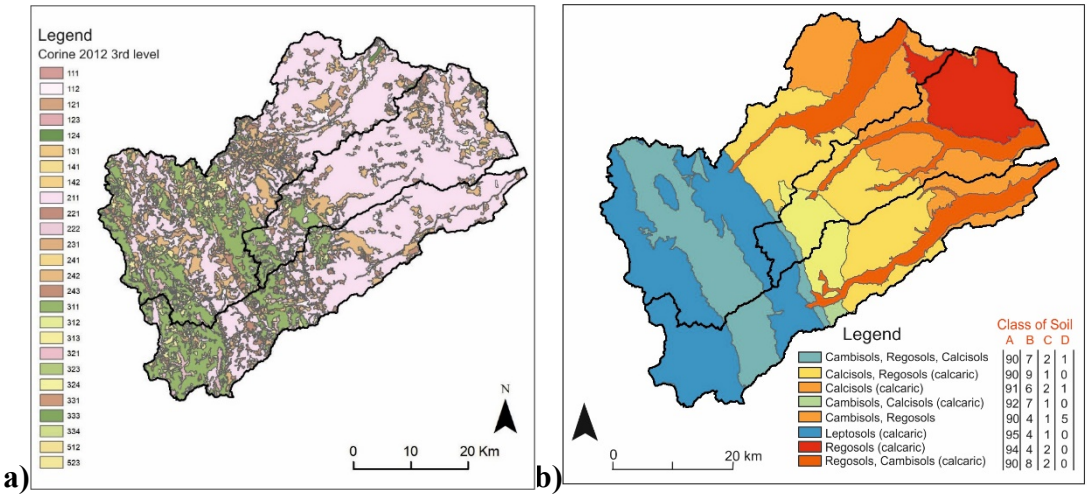

Figure 5. a) Corine Land use map (3rd Level): numbers are reported according to the official legend; b) Soil Classes Map.

All these groups are characterized by dominant calcareous horizons, in line with the geological features of the territory and are usually well-drained soils with fine to medium texture; given their high spatial variability, a further generalization was carried out in order to obtain more homogeneous areas, in agreement with the geomorphological characteristics of the territory (Figure 5b). According to the NRCS (Natural Resource Conservation Service) hydrologic method [14], for each type of soil have been assigned values as a percentage of the Hydrologic Soil Groups classified as follows on the base on their infiltration rate:

- Group A: soils with low runoff potential and high infiltration rate even when thoroughly wetted. They consist mainly of deep, well drained sand or gravel and have a high rate of water transmission (greater than 7.6 mm/hr).
- Group B: soils with moderate infiltration rate when thoroughly wetted and consist of moderately deep to deep, moderately well to well drained soils with moderately fine to moderately coarse textures. They have a moderate rate of water transmission (3.8–7.6 mm/hr).
- Group C: soils with low infiltration rate when thoroughly wetted and consist chiefly of soils with a layer that inhibits downward movement of water and soils with moderately fine to fine texture. They have a low rate of water transmission (1.3–3.8 mm/hr).
- Group D: soils with high runoff potential. They have very low infiltration rate when thoroughly wetted, they may contain a permanent water table and consist of clay soils with a high swelling potential, shallow soils over nearly impervious material and may contain a claypan or clay layer at or near the surface. These soils have a very low rate of water transmission (0–1.3 mm/hr).

2.4. Hydrological modeling

The hydrological model for the study area was realized through two distinct phases. In a former phase, data concerning the morphometry and the hydro-geomorphological characteristics of the river basins (land use, soil type etc) were preprocessed using the tools for ArcGIS "HEC-GeoHMS" version 10.2, developed by the U.S. Army Corps of Engineers [15]. This software allows to process

spatial data to obtain dimensional, morphological and hydrological characteristics of the river basins. These data were subsequently used to perform hydrological simulations through HEC-HMS software v. 4.3, also developed by the U.S. Army Corps of Engineers [16].

The morphological characterization of the river basins through HEC-GeoHMS was carried out using a 1m high-resolution DTM (obtained processing LiDAR images provided by the Italian Ministry of Environment): this allows to disaggregate the three watersheds (Musone, Esino and Potenza) into a series of interconnected sub-basins (50 in total) and to divide the stream networks in reaches and junctions (Figure 6a). Physical characteristics such as the river length and slope, subbasin slope, subbasin centroid location and elevation, longest flow have been also extracted. The evaluation of the hydrological parameters (necessary for the subsequent calculation of infiltration and runoff coefficients in HEC-HMS) was then performed by applying the "Curve Number" method, developed by the Soil Conservation Service of the United States. The method provides the computation of the parameter Curve Number (CN), a dimensionless parameter that ranges between 0 and 100 and expresses the capacity of the soil to produce direct runoff: the higher the value the greater the runoff produced with the same rainfall. A grid file of the Curve Number was obtained by geoprocessing operation in ArcGIS, combining the previously created shapefiles of the land use and of the soil type (Figure 6b).

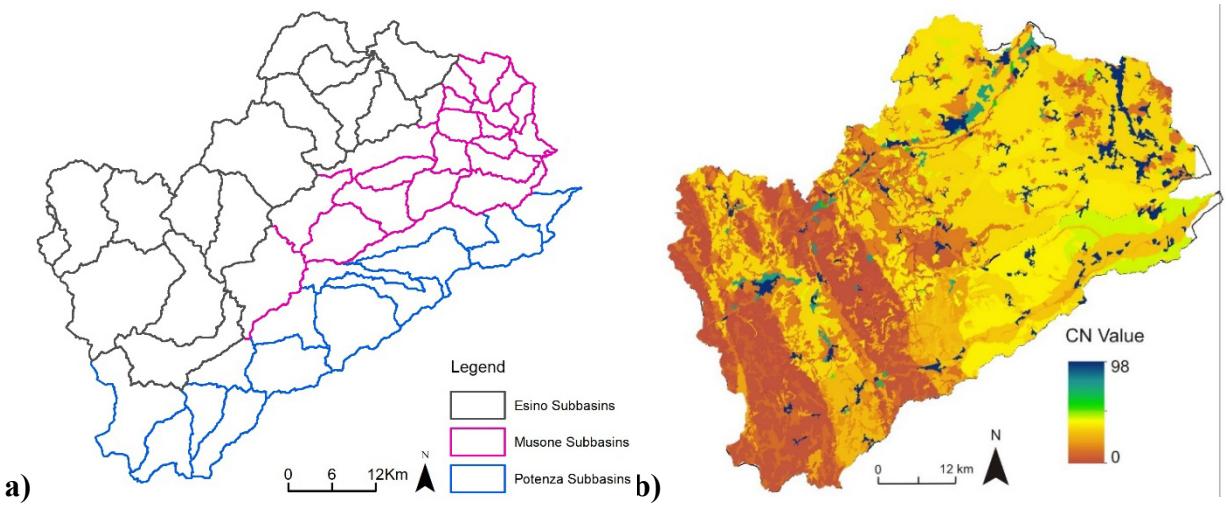

Figure 6. a) HEC-HMS schematization and watershed delineation; different colors indicate different river basins. b) The Curve Number (CN) map of the study area.

The variability in the CN depends on several factors as rainfall intensity and duration, soil moisture conditions, vegetation cover, temperature; these factors are collectively called Antecedent Runoff Conditions (ARCs). ARCs are divided into three classes: II for average conditions, I for dry conditions, and III for wet conditions [17]. Taking into account the purpose of the work, i.e. the runoff computation in critical conditions, the ARCs III were chosen and the initial grid file (corresponding to the ARCs II) was modified according to the following formula:

$$CN(ARCs\ III) = \frac{CN(ARCs\ II)}{0.43 + 0.0057 \times CN(ARCs\ II)} \quad (8)$$

The CN values thus obtained can be considered reliable, as they are in line with those obtained in previous studies through calibration procedures with real events (Materazzi, 2015).

3. Results and discussion

The rainfalls series collected for each of the 18 rain gauges, as described in chapter 2b, have been processed for the construction of the DDF curves for different event durations, return times and length of the time series (Figure 7a). More specifically, for each rain gauge, the analysis was performed on:

- two historical series (1951–2018; 1998–2018)
- five durations (1, 3, 6, 12, 24 hours)
- two return times: 100 yrs (corresponding to an Annual Exceedance Probability—AEP of 1%) and 200 yrs (corresponding to an Annual Exceedance Probability—AEP of 0.5%). The results of this analysis are globally shown in Table 3.

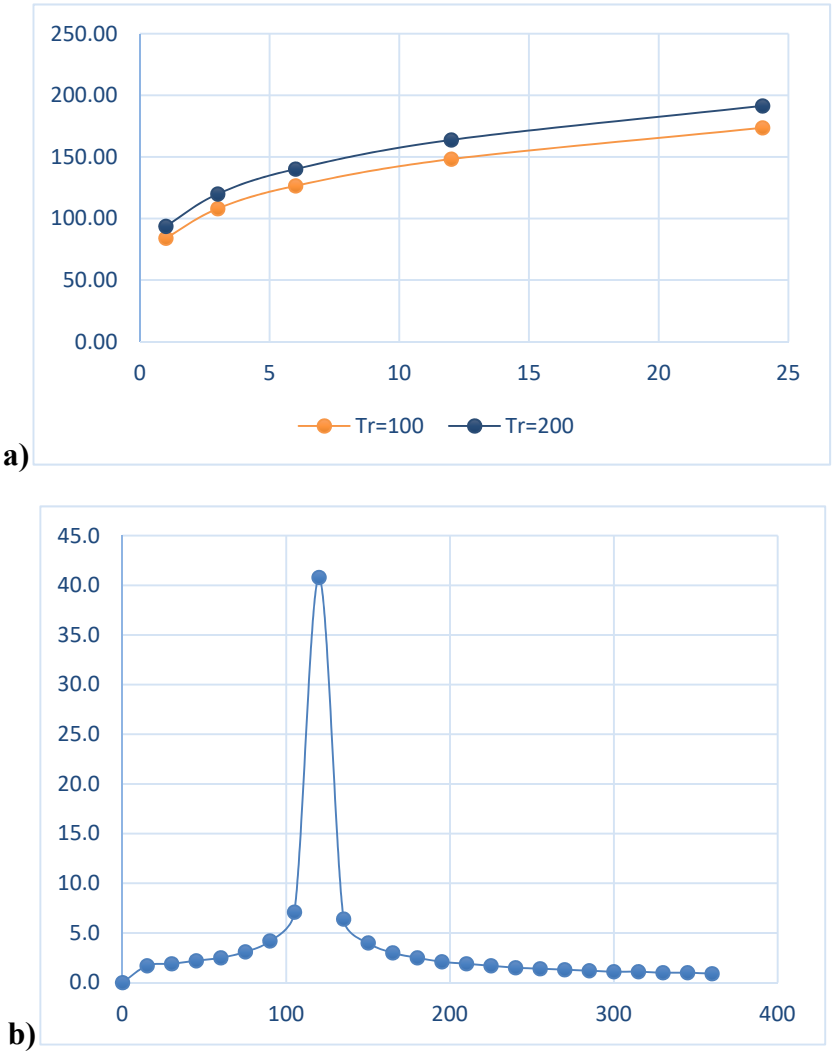

Figure 7. a) DDF curves and b) Chicago-type hyetograph relative to the rain gauge of Senigallia.

For each rain gauge (and consequently for each return time and for both series analyzed) the Chicago-type hyetographs was computed; these hyetographs (Figure 7b) were later used as input within each of the 12 HEC-HMS hydrological models (3 river basins × 2 return times × 2 rainfalls series). The regionalization of the rainfall data, as mentioned in paragraph 2b, was carried out using the Thiessen polygon method.

Table 3. a and n coefficient calculated for different return times and different lengths of the rainfalls series.

1951–2018					1998–2018			
100 years		200 years		Rain Gauge ID	100 years		200 years	
a	n	a	n		a	n	a	N
54.615	0.2988	60.07	0.2982	2039	57.987	0.3155	64.098	0.3132
62.173	0.2575	68.404	0.2552	2038	74.051	0.2687	82.329	0.2663
50.442	0.304	54.828	0.3038	2047	53.943	0.3058	58.695	0.3068
65.038	0.2261	71.92	0.2239	2068	53.572	0.2671	58.574	0.267
77.785	0.2575	87.368	0.2538	2148	90.076	0.2565	101.44	0.252
64.809	0.2812	71.392	0.2802	2149	56.107	0.3069	61.164	0.3071
47.735	0.353	51.951	0.3546	2157	48.678	0.4067	52.839	0.41
63.945	0.2852	70.601	0.2839	2165	74.051	0.2687	82.329	0.2663
62.538	0.2703	69.53	0.2664	2167	66.76	0.2891	73.955	0.2851
84.021	0.2284	93.694	0.225	2105	89.232	0.1889	99.406	0.1846
54.593	0.3454	59.865	0.3457	2144	50.016	0.3578	54.755	0.359
59.104	0.325	65.107	0.3252	2099	52.491	0.3409	57.357	0.3424
58.046	0.2672	64.265	0.2638	2063	71.702	0.1516	79.596	0.1426
88.903	0.2738	99.831	0.2717	2073	98.563	0.2704	110.89	0.2683
54.615	0.2988	60.07	0.2982	2023	57.987	0.3155	64.098	0.3132
56.03	0.2635	61.488	0.261	2143	53.358	0.3164	58.338	0.3156
52.226	0.4392	57.328	0.4432	2067	51.985	0.4723	56.788	0.4787
57.053	0.3628	62.491	0.3617	2124	61.979	0.3396	67.877	0.3369

Once the design storm was developed, the basin model was defined in HEC-HMS. Some data relating to the sub-basins (including the NC), previously calculated in HEC-GeoHMS, were automatically imported into the model. The time of corrective action was instead calculated using the Kirpich Method, developed for small drainage basins in Tennessee and Pennsylvania, with basin areas from 1 to 112 acres

$$Tc = 0.0078L^{0.77}\left(\frac{L}{H}\right)^{0.385} \tag{9}$$

where Tc is the time of concentration in minutes, L is the maximum hydraulic flow length in feet, and H is the difference in elevation in feet between the outlet of the watershed and the hydraulically most remote point in the watershed. Basing on the values obtained, a duration of 6 hours for the design storm of each rain gauge, in line with the time of concentration of all the sub-basins, was chosen. "Net rain" and "rainfall-runoff transformation process" were finally evaluated by applying

the Soil Conservation Service methods, as the SCS Curve Number Loss and the SCS Unit Hydrograph Transform respectively.

Concerning the river reaches the choice of the routing procedure fell on the SCS Lag method, which is best suited for short stream segments with a predicable travel time that doesn't vary with flow depth. Once the data has been entered, the simulation has been started for each of the models provided. The results are shown in Table 4.

Table 4. Flow rate values calculated for different return times and different lengths of the rainfalls series: the fourth column shows the percentage variation of the second series compared to the first.

	Q [m^3/s] 100 yrs 1951–2018	Q [m^3/s] 100 yrs 1998–2018	Variation [%]
Potenza-Subbasin			
W1070	44.7	51.9	16.11
W1080	28.7	25.9	−9.76
W1130	30.6	33.8	10.46
W1180	63.1	61.5	−2.54
W1190	77.5	86.8	12.00
W1280	88.6	105.1	18.62
W1410	18	24.9	38.33
W1500	24.9	32.4	30.12
W1520	48.2	59	22.41
W1610	42.4	56	32.08
W1740	21.5	28.1	30.70
W940	42.1	48.8	15.91
W950	52.6	62.8	19.39
W970	72.9	88.6	21.54
W1070	54.3	62.7	15.47
W1080	34.9	31.4	−10.03
W1130	37.1	40.8	9.97
W1180	75.2	72.9	−3.06
W1190	94	104.7	11.38
W1280	104.4	123.1	17.91
W1410	23.2	31.5	35.78
W1500	32.5	41.3	27.08
W1520	56.5	68.6	21.42
W1610	55.3	71.5	29.29
W1740	27.4	35.4	29.20
W940	51	58.9	15.49
W950	60.9	72.9	19.70
W970	86.1	104.6	21.49

Continued on next page

	Q [m^3/s] 100 yrs 1951–2018	Q [m^3/s] 100 yrs 1998–2018	Variation [%]
Esino-Subbasin			
W1060	67.8	80.7	19.027
W1160	171.3	146	−14.769
W1170	85.5	73.3	−14.269
W1260	106.2	118.3	11.394
W1280	12.6	12.6	0.000
W1290	79.1	77.1	−2.528
W720	18	17.9	−0.556
W730	58.4	48.5	−16.952
W780	29.1	30.5	4.811
W820	26.4	25.7	−2.652
W840	120	104.6	−12.833
W910	100.9	97	−3.865
W930	135.4	160.5	18.538
W940	161.4	177.9	10.223
W950	54.5	44.4	−18.532
W1060	79.3	102.1	28.75
W1160	195.7	164.9	−15.74
W1170	99.9	85	−14.91
W1260	123.6	137	10.84
W1280	16.7	16.4	−1.80
W1290	92.7	90.2	−2.70
W720	22.7	22.2	−2.20
W730	70.7	58.6	−17.11
W780	37.6	39	3.72
W820	34.9	33.6	−3.72
W840	140.5	122	−13.17
W910	116.2	111.3	−4.22
W930	168.4	198.7	17.99
W940	188.9	208.1	10.16
W950	66.3	53.5	−19.31

Continued on next page

	Q [m^3/s] 100 yrs 1951–2018	Q [m^3/s] 100 yrs 1998–2018	Variation [%]
Musone-Subbasin			
W1050	68.6	92	34.11
W1080	72.4	66.3	−8.43
W1100	54.2	44.1	−18.63
W1240	71.6	56.7	−20.81
W1300	64.9	50.1	−22.80
W680	29.7	25.3	−14.81
W690	25.1	22.7	−9.56
W700	26.4	33.5	26.89
W720	36.2	42.2	16.57
W730	17.8	23	29.21
W750	37.5	50.1	33.60
W760	32.0	44	37.50
W800	37.5	53	41.33
W810	26.1	34.1	30.65
W820	34.5	46.6	35.07
W850	32.5	43.2	32.92
W860	63.9	75.6	18.31
W940	52.3	69.5	32.89
W950	55.9	68.2	22.00
W960	56.9	72.9	28.12
W970	66.4	85.3	28.46
W1050	84.2	112.0	33.02
W1080	88.1	80.1	−9.08
W1100	67	54.0	−19.40
W1240	88.7	69.7	−21.42
W1300	82.9	63.9	−22.92
W680	31.4	33.2	5.73
W690	26.4	28.4	7.58
W700	32.1	42.2	31.46
W720	42.2	52.1	23.46
W730	21.8	28.8	32.11
W750	45.8	60.7	32.53
W760	39.9	54.2	35.84
W800	47.6	66.8	40.34
W810	31.4	40.8	29.94
W820	42.4	56.7	33.73
W850	39.8	52.4	31.66
W860	78.3	92.1	17.62
W940	63.6	84.2	32.39
W950	68.4	82.8	21.05
W960	68.1	87.0	27.75
W970	80.6	103.3	28.16

For each basin analyzed, the table shows the list of sub-basins, the flow rate calculated for different return times (100 yrs or 200 yrs) and for the two historical series analyzed (1951–2018 or 1998–2018). The rightmost column, with different colors, indicates the percentage variations (positive or negative) of the flow rate calculated from the most recent rainfall series compared to the longer one. In particular, red color evidences flow rate increase, green color flow rate decrease, yellow color positive or negative deviations not exceeding 10%; this latter value takes into account the uncertainty and the number of rain gauges (not high) used for the statistical analysis.

The analysis of results, clearly shows that most of the Potenza and Musone sub-basins, if modeled using the rainfall series 1998–2018, increases more than 30% the flow rate for both 100 yrs and 200 yrs return times. The Musone river, on the other hand, has a more uncertain behavior. On the other hand, observing the same results in Figure 8a,b (where the areas of the Thiessen polygons are also reported) it is evident that most of the "uncertain" percentage variations (within a range of ±10%) are only associated with 3–4 rain gauges, while those negative essentially to only one. These apparent rainfalls anomalies, once the quality of data coming from these sensors has been verified, will require future climatological insights.

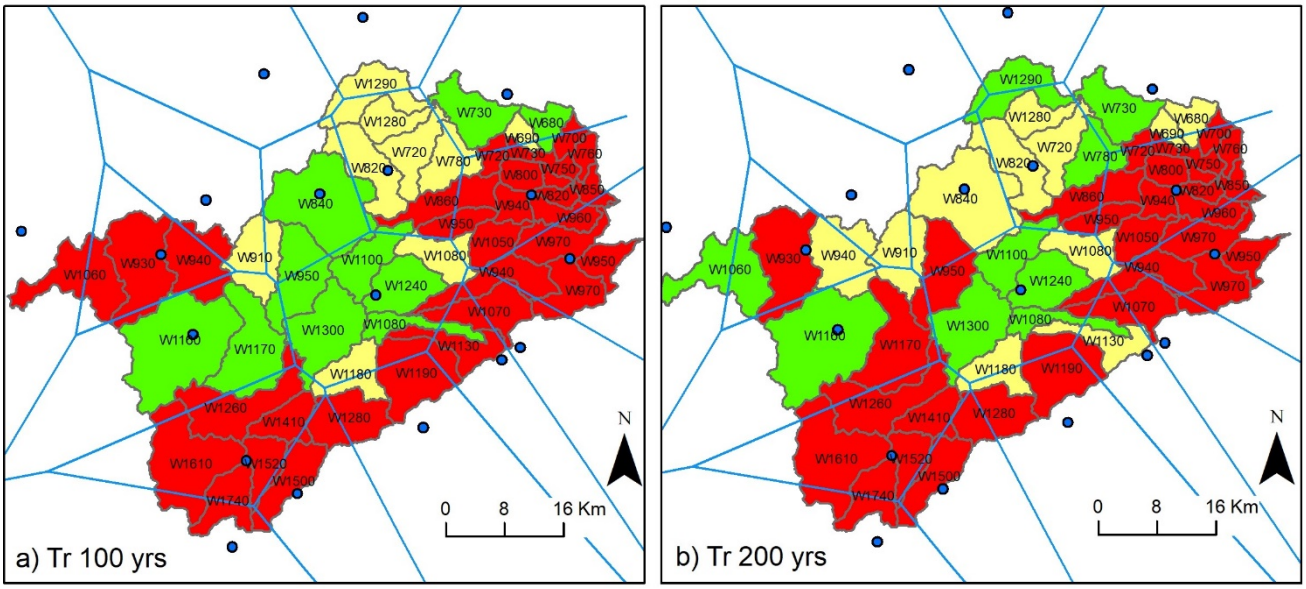

Figure 8. Modeling results: percentage variation between flow rate calculated using 1998–2018 series and 1951–2018 series for a) Tr = 100 yrs and b) Tr = 200 yrs. Red color indicates positive variations (> 10%); green color, negative variations (< −10%); yellow color, no significant variations (between −10% and +10%).

4. Conclusions

The present work, comparing the results of hydrological models derived from statistical analyses of different historical rainfalls series showed that:

- Mann-Kendall and Sen's Slope estimator tests evidenced a positive, although weak and not evenly distributed, positive trend of rainfall starting from 1950; this trend is slightly more evident for the period 1998–2018;

- the DDF curves of 18 pluviometers uniformly distributed in the study area, calculated using a recent rainfalls series (1998–2018), show heights of precipitation significantly higher than those derived from a longer rainfall series (1951–2018) for the return times considered (100 yrs and 200 yrs);
- Chicago-type design storms, calculated from the recent rainfalls series, generate higher flood rates when entered as input data in a hydrological model;
- the hydrological model developed for the study area shows how the flow rate generated by the use of the 1998–2018 pluviometric series is in many cases more than 30% higher than the other;
- values apparently in contrast with those cited are to be associated with the response of few, single sensors whose reliability have to be verified or adequately justified from a climatological point of view;
- the results obtained by the present study, although preliminary and limited to a small sector of central Italy, show that the ongoing ascertained climate change is associated with a change in the rainfall regime, turning towards an increase in rainfall intensity and frequency of extreme events;
- the use of recent but short rainfall series, although less significant from a statistical point of view, can therefore be more reliable if included in a numerical modeling for the definition of future risk scenarios.

Acknowledgments

The authors want to thank Consorzio di Bonifica delle Marche for kindly providing all the data.
ORCID:
Margherita Bufalini: https://orcid.org/0000-0003-3278-7058
Marco Materazzi: https://orcid.org/0000-0002-9480-5680

Conflict of interest

No potential conflict of interest was reported by the authors.

References

1. Masson-Delmotte V, Zhai P, Pörtner H, et al. (2018) An IPCC Special Report on the impacts of global warming of 1.5 °C above pre-industrial levels and related global greenhouse gas emission pathways, in the context of strengthening the global response to the threat of climate change, sustainable development, 24.
2. Huong HTL, Pathirana A (2013) Urbanization and climate change impacts on future urban flooding in Can Tho city, Vietnam. *Hydrol Earth Syst Sci* 17: 379–394.
3. Sperotto A, Torresan S, Gallina V, et al. (2016) A multi-disciplinary approach to evaluate pluvial floods risk under changing climate: The case study of the municipality of Venice (Italy). *Sci Total Environ* 562: 1031–1043.
4. Amici M, Spina R (2002) *Campo medio della precipitazione annuale e stagionale sulle Marche per il periodo 1950–2000*, 103.

5. Gentilucci M, Bisci C, Burt P, et al. (2018) *Interpolation of Rainfall through Polynomial Regression in the Marche Region (Central Italy)*, Springer International Publishing.
6. Pierantoni P, Deiana G, Galdenzi S (2013) Stratigraphic and structural features of the sibillini mountains(Umbria- Marche Apennines, Italy). *Ital J Geosci* 132: 497–520.
7. Gumbel EJ (1941) Probability-interpretation of the observed return-periods of floods. *Eos, Trans Am Geophys Union* 22: 836–850.
8. Gumbel EJ (1954) Statistical theory of extreme values and some practical applications. *Appl Math Ser* 33: 341–342.
9. Tabari H, Talaee PH (2011) Analysis of trends in temperature data in arid and semi-arid regions of Iran. *Glob Planet Change* 79: 1–10.
10. Gocic M, Trajkovic S (2013) Analysis of changes in meteorological variables using Mann-Kendall and Sen's slope estimator statistical tests in Serbia. *Glob Planet Change* 100: 172–182.
11. Thiessen AH (1911) Precipitation for large areas. *Mon Weather Rev* 39: 1082–1084.
12. NBGC (2006) Valter Sambucini, Ines Marinosci, *CORINE LAND COVER 2006 (ISPRA)*.
13. Food and Agriculture Organization of the United Nations (2015) *International soil classification system for naming soils and creating legends for soil maps.*
14. USDA-NRCS (2009) National Engineering Handbook Chapter 7: Hydrologic Soil Groups. *Part 630 Hydrol Natl Eng Handb*, 5.
15. Fleming MJ, Doan JH (2013) *HEC-GeoHMS geospatial hydrologic modeling extension*.
16. Scharffenberg B, Bartles M, Brauer T, et al. (2018) *Hydrologic Modeling System User's Manual*.
17. USDA-NRCS (2009) Hydrology National Engineering Handbook Chapter 10 Estimation of Direct Runoff from Storm Rainfall. *Part 630 Hydrol Natl Eng Handb.*

AIMS Press